Materials Research. 2025; 28:e20240350
DOI: https://doi.org/10.1590/1980-5373-MR-2024-0350

Uncertainty Quantification in Masses of Alloy Components and Atomic Radii Modification in High-Entropy Alloys Design: Thermophysical Parameters Calculation Approach

***Raphael Basilio Pires Nonato*[a,b]*, *Thomaz Augusto Guisard Restivo*[a], *José Carlos Machado Junior*[a]**

[a]*Universidade de Sorocaba (UNISO), Programa de Pós-Graduação em Processos Tecnológicos e Ambientais, Sorocaba, SP, Brasil.*
[b]*Instituto Federal de Santa Catarina (IFSC), Chapecó, SC, Brasil.*

Received: August 15, 2024; Revised: December 06, 2024; Accepted: January 13, 2025

Given the vast universe of high-entropy alloys (HEAs), solid solution formation (SSF) prediction is increasingly relevant. The processing route leads to uncertainty in the mass of each alloy component, affecting SSF. Furthermore, investigations led to atomic radius modification under interaction with neighboring atoms, also influencing SSF. Therefore, this paper presents an uncertainty quantification framework implemented over the thermophysical parameters calculation (TPC) approach to verify the behavior of the SSF parameters as the mass of the alloy components vary and the atomic radii are modified. The AlCrFeMoNbTaTiVW alloy was subjected to this framework, being the tungsten mass the most influential, and tantalum the less influential overall. Moreover, the atomic radii modification does not work properly under TPC theory, implying in non-SSF prediction even when a solid solution is formed. Thenceforth, equimolar HEAs are now near-equimolar, and the SSF parameters may indicate that some samples of the same alloy batch may result in SSF, others not.

Keywords: *High-entropy alloys (HEAs), uncertainty quantification (UQ), thermophysical parameters calculation (TPC), atomic radii modification, multicomponent alloys.*

1. Introduction

New materials have been developed since ancient times by civilization[1]. The development of materials has been one of the major drivers of evolution. New metals were discovered, and new metal alloys fabricated to solve several key issues in the most diverse areas. It is well known that the mechanical properties of pure metals can be enhanced by alloying each one with other metals or non-metallic elements[1]. In view of this, metal alloys have been based on one principal element for a long time, e.g. iron in steel. Thenceforth, to improve properties, metal alloys were then proposed with two main elements[2].

Posteriorly, the multicomponent alloys, which contain three or more main elements, were then created. Despite their useful properties, in several situations, they may form intermetallic compounds (IM) with complex microstructures corresponding to mechanical properties of undesired magnitudes. Consequently, a novel alloy design paradigm was introduced about two decades ago[3,4]. The related concept involves the mixing of multiple elements in an equimolar or near-equimolar composition. Therefore, the so-called high-entropy alloys (HEAs)[3] emerged, in which their design is based on at least five main elements (concentrations varying between 5 and 35% in molar terms). This denomination is due to their high configurational entropy in the solidification process, promoting random solid solutions, in contrast to complex phases. HEAs represent a new research field within multicomponent alloys and have great potential to combine properties uniquely to enable new engineering applications or enhance the possibilities in existing ones.

This promising research field is being increasingly investigated due to reports of high strength[5], hardness[6,7], ductility[8], fracture and impact toughness[9], corrosion resistance[10], strength-ductility trade-off[11], strength-to-weight ratio[12], low cost of manufacturing[13], among other properties. Variations in HEAs' nomenclature emerged as the topic discussions were addressed, such as RHEAs (refractory)[14], SPHEAs (single phase)[15], LWHEAs (lightweight)[12], among others. Inside the universe of possible HEAs (which commonly has two or more different phases, some of them being IM), in a few cases, a stabilized microstructure consisting of either (a) random solid solution with a simple crystal structure (BCC, FCC, or HCP), or (b) duplex microstructure (two simple solid solutions), which provides more interesting properties to turn into materials for demanding applications. The stabilized solid microstructure normally addresses ductility concomitantly with solid solution hardening. Conversely, whereas adding more elements increases the configurational entropy of a solid solution, the probability of IM formation also augments[16,17].

In this regard, the formation of random solid solutions in HEAs is due to the four core effects: (a) high entropy, (b) sluggish diffusion, (c) lattice distortion, and (d) cocktail[18]. The high-entropy effect occurs due to a high configurational entropy at elevated temperatures. In this condition, the Gibbs free energy of mixing is minimized (per the second law of thermodynamics), thus benefiting the dissolution of IMs[19]. The sluggish diffusion effect is due to lattice distortion,

*e-mail: raphaelbasilio@gmail.com

which provides a slow rate of atomic diffusivity[20]. The lattice distortion effect is caused by introducing substitutional solute atoms into a solvent matrix, displacing the atoms from their theoretical lattice positions[21]. The cocktail effect refers to the interaction between the elements, causing a synergistic blend of properties, such as strength-to-ductility ratio, strength-toughness balance, fatigue resistance, and corrosion resistance, among others[22].

Therefore, three possible states are the result of HEAs obtainment: (a) elemental phases, which is a solid solution based on only one element; (b) IM, a stoichiometric compound with specific superlattices; and (c) solid solution, in which a complete or an almost complete mixing of all the elements in the form of BCC (body-centered cubic), FCC (face-centered cubic), or HCP (hexagonal close-packed).

Since the first investigations in the field of HEAs, the prediction of phase formation and composition is one of the most reported branches in the specific literature[23-25]. In this regard, there are four main approaches commonly applied in this type of alloy design: (a) molecular dynamic (MD) simulations[26,27]; (b) calculation phase diagrams (CALPHAD)[28,29]; (c) machine learning[30]; and (d) thermophysical parameters calculation (TPC)[31,32].

The TPC approach (applied in this work) addresses the calculation of several parameters and the evaluation of the corresponding criteria that, theoretically, if attended, refers to random solid solutions. The selected set of parameters and criteria is applied in each alloy design to predict solid solutions and phases. In this work, 8 parameters and their corresponding criteria are calculated according to their relevance and availability related to the thermodynamic data of the elements.

2. Thermophysical Parameters Calculation (TPC) for HEAs' Design

This section describes the classical TPC (without radii modification), the modified TPC (with radii modification), and the thermophysical parameters and their associated criteria.

2.1. Classical TPC (without radii modification)

The core concept intrinsic to the utilization of the parameters in TPC relies on minimizing the differences in physical and thermodynamic properties of the main elements that constitute the HEAs, conducting to the formation of random solid solutions, thus lowering the likelihood of precipitation of ordered IM or amorphous structures. Although the detailing degree of TPC is low due to not providing information about the phase diagrams, it is a relatively fast method if the objective is only to predict solid solution formation (SSF).

As far as this research could reach, there are at least 29 parameters available in the specific literature[33]. Among them, there are means and standard deviations (e.g. mean melting temperature, standard deviation of density, etc.). Due to report frequency, simplification, and objectives of the analysis, in this paper, 8 parameters and their associated criteria are presented. These criteria provide statuses about the SSF. The application of TPC may predict if a specific combination of elements results in a random SSF or not (e.g. IM, metallic glass, etc.).

This approach does not demand experimental data in what refers to solid solution prediction, besides having a high predictive capacity. Conversely, as a large design space is often required, the referred approach requires a high computational cost. The classical TPC relies on the hard-sphere model atom, which describes the atoms and molecules as solid spheres with no internal structure and no change in radii of the elements involved[34].

2.2. Thermophysical parameters and their associated criteria

Eight parameters and their associated criteria are presented in this paper. The first 2 depend exclusively on the radii of the elements involved; the third depends simultaneously on the radii and masses of the alloy components. The remaining parameters are dependent only on the masses of the alloy components.

Atomic radii difference, $\Delta r(\%)$, (radius dependent): it is defined by the difference between the largest (r_L) and smallest (r_S) atomic radii of the elements involved related to r_L (Equation 1). The first rule of Hume-Rothery addresses that SSF effectively occurs when this difference is lower than 15% (Equation 2)[34].

$$\Delta r(\%) = \frac{r_L - r_S}{r_L} 100. \tag{1}$$

$$SSF : \Delta r(\%) < 15. \tag{2}$$

Topological discrepancy, γ, (radius dependent): it quantifies the non-linear impact of the largest and smallest atoms in SSF. γ is defined as the result of the Fermi level being close to a van Hove singularity in the density of states (Equation 3), where r_M is the mean atomic radius[35]. The criterion for SSF states that the parameter should be smaller than 1.175 (Equation 4):

$$\gamma = \left(1 - \sqrt{\frac{(r_L - r_M)^2 - r_M^2}{(r_L - r_M)^2}}\right) \Big/ \left(1 - \sqrt{\frac{(r_S - r_M)^2 - r_M^2}{(r_S - r_M)^2}}\right). \tag{3}$$

$$SSF : \gamma < 1.175. \tag{4}$$

Polydispersion of atomic radii or atomic size mismatch, δ(%), (radius and molar fraction dependent): it is the mean square deviation of the atomic radii involved (Equation 5) and directly influences the atomic packing, where f_i is the molar fraction of the i-th element involved in the solid solution, and n is the number of alloy components. The associated criterion to SSF is expressed in Equation 6 (with rare exceptions)[36]. The consequence of bond distortion is a corresponding degree of strain[37]. In other words, δ is a manner to quantify the deviation from the ideal lattice.

$$\delta(\%) = \sqrt{\sum_{i=1}^{n} f_i \left(\frac{1 - r_i}{r_M}\right)^2}\, 100. \tag{5}$$

$$SSF : \delta(\%) < 6.5. \tag{6}$$

Mean valence electron concentration or valence electronic configuration, V_M, (molar fraction dependent): it is related to the third rule of Hume-Rothery, that states that elements with

the same type of crystalline structure may form extensive series of solid solution[38]. V_M, representing the mean periodic table group number, is given by Equation 7, where V_i is the electron concentration value of the i-th alloy element. The criterion associated to V_M is that BCC structure is formed when $V_M < 6.87$, and FCC structure when $V_M \geq 8$; otherwise, FCC predominantly occurs, however BCC may occur in some circumstances (Equation 8).

$$V_M = \sum_{i=1}^{n} f_i V_i. \tag{7}$$

$$SSF: \begin{cases} V_M \geq 8, \ FCC, \\ V_M < 6.87, \ BCC, \\ 6.87 \geq V_M \leq 8, \ FCC \, or \, BCC. \end{cases} \tag{8}$$

Entropy of mixing or configurational entropy, ΔS_{MIX}, (molar fraction dependent): the entropy of mixing of the elements involved is expressed by Equation 9 from Boltzmann's hypothesis[39], where R = 8.314 J / mol K is the universal gas constant. The value of ΔS_{MIX} determines the degree of entropy of the alloy, i.e. low-entropy alloys (LEAs) correspond to $\Delta S_{MIX} < 0.69$ R, medium-entropy alloys (MEAs) refer to $0.69 \text{ R} \leq \Delta S_{MIX} \leq 1.61$ R, and HEAs to $\Delta S_{MIX} \geq 1.61$ R. Therefore, $\Delta S_{MIX} \geq 1.61$ R (13.38 J / mol / K) addresses an increasing likelihood to SSF[40], representing the associated criterion (Equation 10). However, concomitantly with a higher value of δ, the opposite tendency is observed, leading to IM formation[41].

$$\Delta S_{MIX} = -R \sum_{i=1}^{n} f_i \ln(f_i). \tag{9}$$

$$SSF: (11 \leq \Delta S_{MIX} \leq 19.5) J / kmol. \tag{10}$$

Electronegativity difference, Δχ, (molar fraction dependent): it is the difference in electronegativities by Pauling, and it leads to a quantification of phase separation and new phase formation[42]. In this regard, this parameter represents the standard deviation of electronegativity, i.e. the fourth rule of Hume-Rothery (Equation 11), in which χ_i is the electronegativity of the i-th element, and χ_M is the mean of the electronegativity of the elements involved. Values of electronegativity difference lower than 6% correspond to SSF, as per Equation 12.

$$\Delta\chi(\%) = \sqrt{\sum_{i=1}^{n} f_i (\chi_i - \chi_M)^2}\, 100. \tag{11}$$

$$SSF: \Delta\chi(\%) < 6. \tag{12}$$

Average mixing enthalpy, ΔH_{MIX}, (molar fraction dependent): governed by the regular solution model[43], i.e. Equation 13, where c_i and c_j are the normalized fractions of the i-th and j-th elements (Equation 14 and Equation 15, respectively), nC_2 is the number of atomic pairs, and $\Delta H_{ci,cj}$ is the mixing enthalpy of binary liquid alloys formed by the i-th and j-th elements (stated in Equation 16), where Ω_k is the k-th factor of third order approximation polynomial (obtained by Miedema's scheme, via thermodynamic tables for each atomic pair[43]. The associated criterion for SSF is shown in Equation 17.

$$\Delta H_{MIX} = \sum_{i=1; i \neq j}^{nC_2} \Delta H_{c_i, c_j}. \tag{13}$$

$$c_i = \frac{f_i}{f_i + f_j}. \tag{14}$$

$$c_j = \frac{f_j}{f_i + f_j}. \tag{15}$$

$$\Delta H_{c_i, c_j} = 4 c_i c_j \left(\sum_{k=0}^{3} \Omega_k (c_i - c_j)^k \right). \tag{16}$$

$$SSF: (-22 \leq \Delta H_{MIX} \leq 7) kJ / mol. \tag{17}$$

Entropy-enthalpy relation or interacting parameter, Ω, (molar fraction dependent): The relation between enthalpy and entropy is employed to predict the phase formation, especially for HEAs. The introduction of Ω is to verify the contribution of entropy of mixing in the SSF. The parameter and its associated criterion are calculated by Equation. 18, and Equation 19, respectively[38], where T_M is the mean temperature.

$$\Omega = \frac{T_M \, \Delta S_{MIX}}{|\Delta H_{MIX}|}. \tag{18}$$

$$SSF: \Omega > 1. \tag{19}$$

2.3. Modified TPC (with radii modification)

Regarding the modified TPC approach, 3 of the 8 parameters presented herein include the atomic radii of the elements involved in their formulation. The classical TPC approach in HEAs' design assumes that the atomic radii of the elements involved are invariable, as when dealing with pure metals. However, in alloys, several investigations stated that a change in the local electronic environment occurs, suggesting a change in atomic radii[44]. This type of alteration is based on the soft sphere model and is significant to the development of amorphous, crystalline, and IM because the radii modification impacts the lattice distortion[45], thus affecting the alloy properties. Therefore, the 3 topological parameters of HEAs and their associated criteria addressed herein are calculated by observing 2 distinct situations: (a) per classical TPC: atomic radii as those in pure elements (no modification in atomic radii); and (b) per modified TPC: atomic radii as those in alloys (with atomic radii modification). The impact of radii modification on HEAs is evaluated by comparing the results without and with radii modification. Both situations, which are subjected to uncertainty in the masses of the alloy components involved, are calculated via a specific code developed in Matlab®. In this regard, the formulated code was based on one previously developed in Microsoft Visual Basic®[46].

As previously proposed[46], the atomic radius of the i-th element in the solution is modified according to Equation 20, in which the prime indication addresses its modified radius, E_i is the electronic shell number of the i-th element, and E_M is the mean electronic shell number. In the context of uncertainty, it is important to note that the uncertainty in mass also originates the uncertainty in the condition of modified

radii of the elements due to involving the means of both electronic shell number and valence electron concentration.

$$r_i^{'} = r_i\left[\left(\frac{E_M}{V_M}\right)/\left(\frac{E_i}{V_i}\right)\right]. \quad (20)$$

3. Uncertain Modeling of Aleatory-type Variable

This section describes the possible types and sources of uncertainty, besides the mathematical model of aleatory-type one. Moreover, the uncertainty quantification process is highlighted, with its input and response quantities.

3.1. Sources and types of uncertainty

Uncertainty is inherent to the most varied engineering applications. Materials, processes, assumptions, conditions, simplifications, etc. are some of the main focuses when investigating sources of uncertainty. The engineering decision-making processes often demand uncertainty quantification (UQ) analyses, in which full detail of the uncertainty is required. Uncertainty generally originates from the following sources: (a) model form (mathematical modeling, simplifications, assumptions, among others); (b) model input (input data, surroundings, restrictions, etc.); and (c) numerical approximation (domain discretization, number of algebraic operations, etc.)[47]. In predictions based on mathematical models, the classification of uncertainties can be listed as the following: (a) epistemic: corresponds to a lack of knowledge about the behavior of the variable, which is commonly represented by an interval[47]; (b) aleatory: variability inherent to the system behavior, which can be better represented and quantified, however not eliminated. The aleatory-type can be represented by a probability density function (PDF) and/or a cumulative density function (CDF)[48]; and (c) mixed: a combination of both epistemic- and aleatory-type ones, which can be represented by a PDF and/or a CDF with an interval[49]. This paper deals with the aleatory type only.

3.2. Aleatory-type uncertainty

The adoption of the aleatory-type uncertainty refers to the nature of the manufacturing route adopted for this HEA, as if it were on its specific production line. In view of this, the Gaussian model was selected in this paper. Regarding this type of uncertainty, the information generally comes from a candidate, selected, available, or known PDF and/or CDF. If n_k is the number of known parameters of the PDF of the i-th probabilistic uncertain input quantity (UIQ) X_i, k is the k-th known parameter, and the PDF of X_i is represented by $f_{Xi}(x_i, x_{i+1}, \ldots, k, \ldots, n_{k-1}, n_k)$, then the realizations of X_i are obtained from the inverse function of the PDF, as per Equation 21, in which x_i is a possible outcome from a set χ_i containing all possible outcomes. Therefore, the CDF F_{Xi} can be attributed to every element x_i such that both conditions are concomitantly fulfilled (Equation 22 and Equation 23):

$$x_i = f_{X_i}^{-1}\left(x_i, x_{i+1}, \cdots, k, \cdots, n_{k-1}, n_k\right). \quad (21)$$

$$\sum_{x_i \in \chi_i} F_{X_i}\left(x_i, x_{i+1}, \cdots, k, \cdots, n_{k-1}, n_k\right) = 1. \quad (22)$$

$$F_{X_i}\left(x_i, x_{i+1}, \cdots, k, \cdots, n_{k-1}, n_k\right) \in \left[0, 1\right], \forall\, x_i \in \chi_i. \quad (23)$$

3.3. Uncertainty quantification (UQ), uncertain input quantities (UIQs), and system response quantities (SRQs)

In the context of model-based predictions, between the real situation and the mathematical model selected to represent it there is a gap that partially originates the uncertainty. Initial and boundary conditions, analysis time, logical complexity, errors, rounding, multiplicative factors, among others, originate the uncertainty[47].

In view of safety and functionality issues, the impact of these sources of uncertainty should be investigated and predicted[50], starting by designating these sources as UIQs (with known parameters to define the corresponding PDF and/or CDF).

These UIQs should be propagated throughout the selected mathematical model to obtain the SRQs. Among the available uncertainty propagation methods, Monte Carlo sampling (MCS) is one of the most widely used[51]. Other relevant methods are also applied: quasi-Monte Carlo sampling (QMCS)[52], subset simulation (SS)[53], polynomial chaos (PC)[54], fuzzy interval arithmetic (FIA)[55], analytical uncertainty propagation (AUP)[56], Latin hypercube sampling[57] (LHS, applied in this work), among others. The adoption of LHS is explained by the ratio of ease of implementation and computational cost, thus demanding reasonable sample sizes to converge.

Each UIQ or SRQ is represented by a column vector $\mathbf{V_i}$ in the form of Equation 24, where p is the p-th realization, the superscript between parentheses is the realization number, n_r corresponds to the number of realizations, and $\mathbb{N}$ is the closed set of natural numbers.

$$\boldsymbol{V_i} = \left[v_i^{(1)}, v_i^{(2)}, \cdots, v_i^{(p)}, \cdots, v_i^{(n_r-1)}, v_i^{(n_r)}\right]^T,\ p \in \mathbb{N} | 1 \le p \le n_r. \quad (24)$$

Thenceforth, for each alloy, the mathematical model $\mathcal{M}$ that maps the n UIQs ($\mathbf{X_1}$, $\mathbf{X_2}$, …, $\mathbf{X_n}$) addressed in this work (mass of each alloy component involved) into the p SRQs ($\mathbf{Z_1}$, $\mathbf{Z_2}$, …, $\mathbf{Z_p}$) is presented in Equation 25. It is important to note that, given the uncertainty in the process, a previous equimolar HEA turns out now to have a near-equimolar composition.

$$\mathcal{M}\left(\boldsymbol{X}_1, \boldsymbol{X}_2, \cdots, \boldsymbol{X_n}\right) \rightarrow \boldsymbol{Z}_1, \boldsymbol{Z}_2, \cdots, \boldsymbol{Z_p}. \quad (25)$$

In addition, within the scope of this paper, a variable can be regarded as a deterministic quantity if: (a) its variation can be neglected; (b) the computational cost to include it in the uncertainty framework is prohibitive; (c) its value is known exactly; or (d) its variation is of low relevance to the objective of the analysis.

4. Example

The numerical example addressed in this paper refers to a 9-distinct-element alloy, AlCrFeMoNbTaTiVW, with a body-centered cubic (BCC) structure, named metallic diamond alloy 6, reported in[7]. Aiming at maximizing the alloy hardness, the manufacturing route of the alloy was the

following: (a) powder mixing; (b) powder compaction; (c) arc plasma melting (casting); and (d) annealing[7].

4.1. Problem description

Some of the input data of the elements involved in the alloy theoretical composition comes directly from the periodic table of elements, and the remaining data are from the literature already mentioned in the section concerning the thermophysical parameters and the associated criteria[7,34-46,58].

The uncertainty in mass proposed by this investigation refers to the following manufacturing conditions: (a) the mass of each alloy component is rounded in the stage of separation and weighing of the 9 distinct raw powder, which represents the minor loss of mass; (b) there is a loss of mass during the compaction process of the raw powder, which also represents a low degree of mass loss; and (c) the major loss occurs in the casting process, significantly explained by the elements with relatively low vapor pressure, and adhesion to the interacting apparatus.

4.2. Uncertainty quantification framework

In an uncertain context, the classical TPC and the modified TPC are both applied to compare the thermophysical parameters without and with radii modification, respectively, to check if they attend the associated criteria to SSF. Therefore, the mass of each alloy component involved can be represented by the mathematical structure of a UIQ. The entire UQ process applied throughout this work is presented in Figure 1, where a flowchart indicates the steps followed.

According to Figure 1, the Gaussian mathematical model is attributed to the mass of each alloy component involved. An estimation of the uncertainty in the UIQs is made and propagated (via LHS) through both classical and modified TPC methods to predict SSF. The SRQs are quantified via the two distinct methods, and, finally, the information on SRQs obtained from both approaches are compared.

Table 1 presents the mean and standard deviation values of each UIQ in this paper. The deterministic mass value of each alloy component involved is assumed as the mean of the simulated probability distribution, whereas the standard deviation is 0.5% of the corresponding mean (partially justified by measurements comparing the outlet mass with the inlet mass). The sample deterministic mass of the alloy is defined as 20 g and 1 x 10^5 realizations are performed. All the calculations and plots reported were performed in MATLAB®. The LHS was implemented using a distinct seed number for each sample generated.

5. Results and Discussion

This section presents the calculation and discussion about the output for the problem of prediction of SSF of the alloy AlCrFeMoNbTaTiVW. This includes probabilistic distributions, graphical sensitivity analyses, relative errors, and Pearson correlation coefficients of the parameters dependent: (a) exclusively on the mass of each alloy component involved; (b) only on the atomic radius of each alloy component involved; and (c) on both mass and atomic radius.

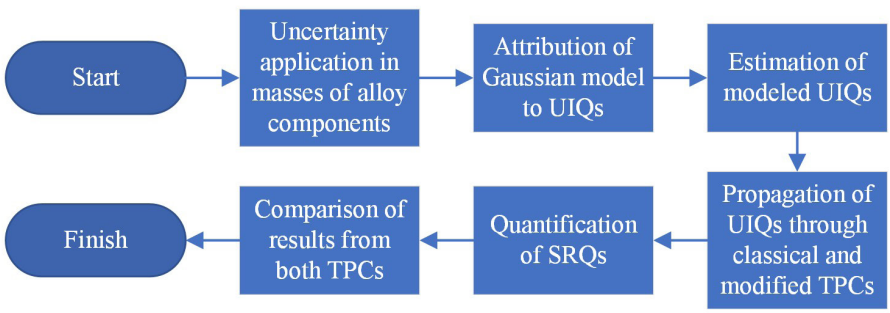

Figure 1. Flowchart of the uncertainty quantification process employed in this work.

Table 1. Input data for the elements involved in the alloy AlCrFeMoNbTaTiVW related to the UQ process.

UIQ	Deterministic value and mean (g)	Standard deviation (% of the mean)
m_{Al}	0.685	0.5
m_{Cr}	1.321	0.5
m_{Fe}	1.419	0.5
m_{Mo}	2.438	0.5
m_{Nb}	2.360	0.5
m_{Ta}	4.597	0.5
m_{Ti}	1.216	0.5
m_{V}	1.294	0.5
m_{W}	4.670	0.5

5.1. Distributions for the UIQs and SRQs

The histogram, PDF, and CDF of the powder mass of the alloy are presented in Figure 2, Figure 3, and Figure 4, respectively, (in blue) aiming to illustrate its shape, dispersion, and convergence to the means of the UIQs to assure an adequate input to be propagated through the mathematical model. Regarding the legends of Figure 2, powder mass is represented by m_p, "DETERM." is the deterministic value (and initial mean) of the parameter (represented by a vertical continuous red line), and "MEAN" is the simulated mean of the parameter after the simulation (vertical continuous green line). The graphical coincidence of both vertical lines indicates the convergence of the mean of m_p with a relative error of 3 x 10^{-7}%.

Among the 8 parameters addressed in this paper, V_M is selected to represent those which depend exclusively on the mass of each alloy component involved. The PDF and CDF of this SRQ are shown in Figure 5 and Figure 6, respectively. γ is chosen to represent those parameters with only atomic radius dependence (Figure 7 and Figure 8), and δ is selected to represent the parameter concomitantly dependent on radius and mass (Figure 9 and Figure 10). In Figure 7 through Figure 10, although calculated, the deterministic values of γ and δ (without radius modification), respectively, are suppressed for means of clarification (they are far from the values covered by the distributions). In view of this, the "DETERM." label represents the modified deterministic value of the referred parameter.

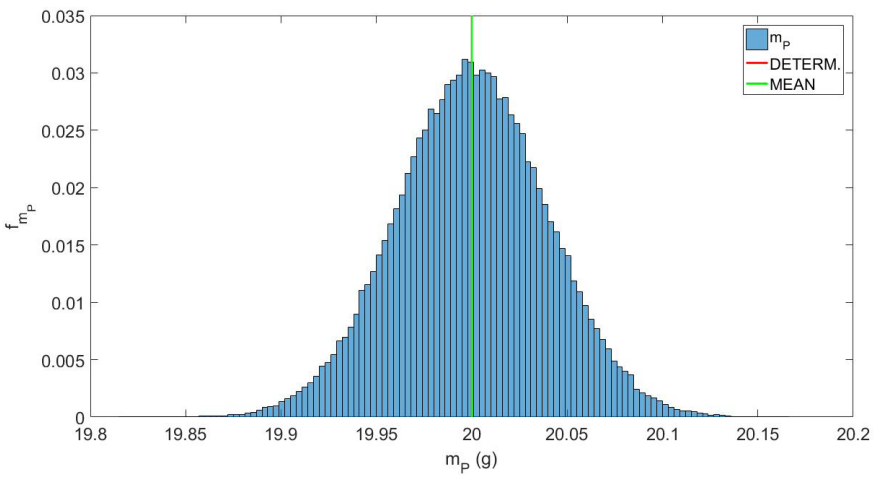

Figure 2. Histogram of AlCrFeMoNbTaTiVW powder mass.

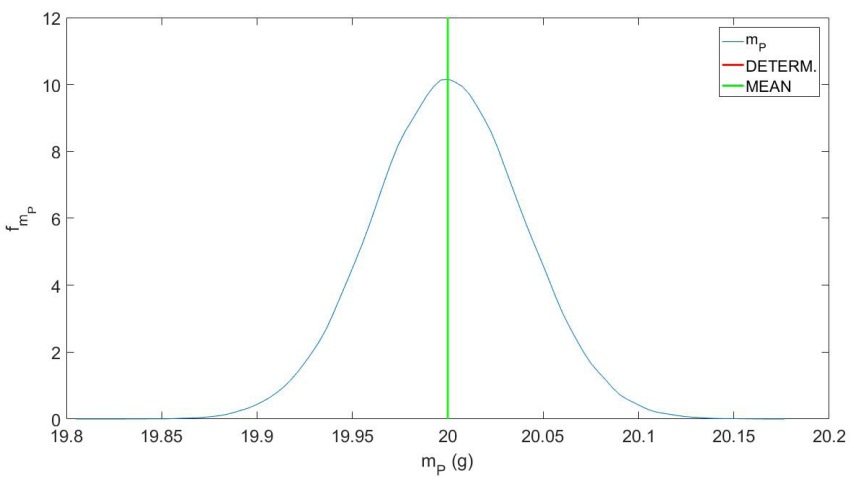

Figure 3. PDF of AlCrFeMoNbTaTiVW powder mass.

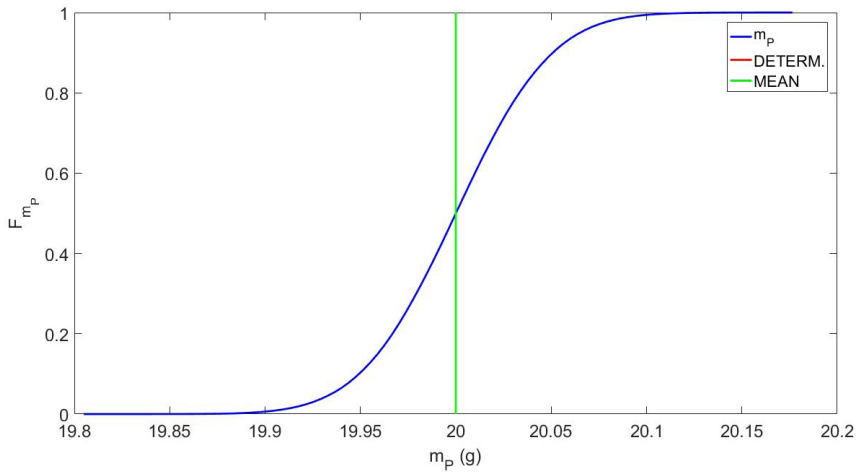

Figure 4. CDF of AlCrFeMoNbTaTiVW powder mass.

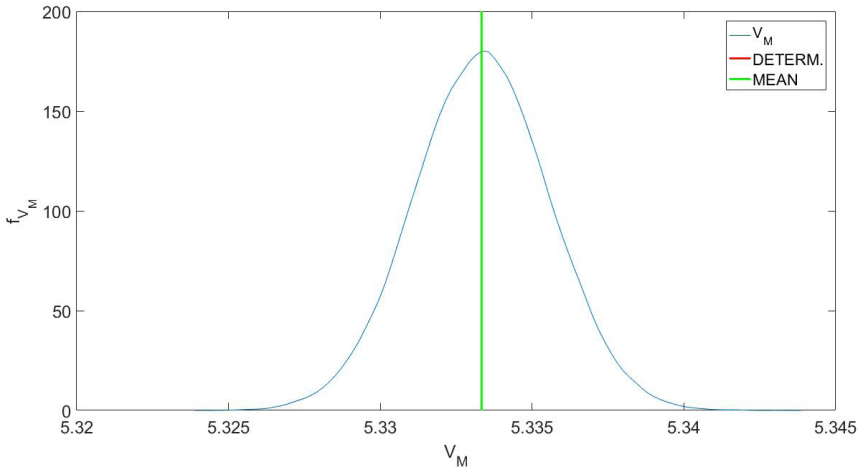

Figure 5. PDF of AlCrFeMoNbTaTiVW mean valence electron concentration (V_M), where "DETERM." stands for the deterministic value of V_M, and "MEAN" for the mean of V_M.

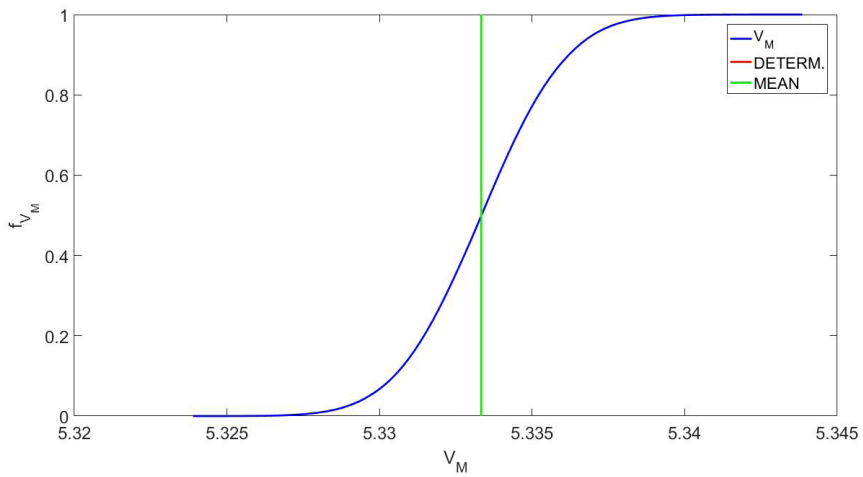

Figure 6. CDF of AlCrFeMoNbTaTiVW mean valence electron concentration (V_M), where "DETERM." stands for the deterministic value of V_M, and "MEAN" for the mean of V_M.

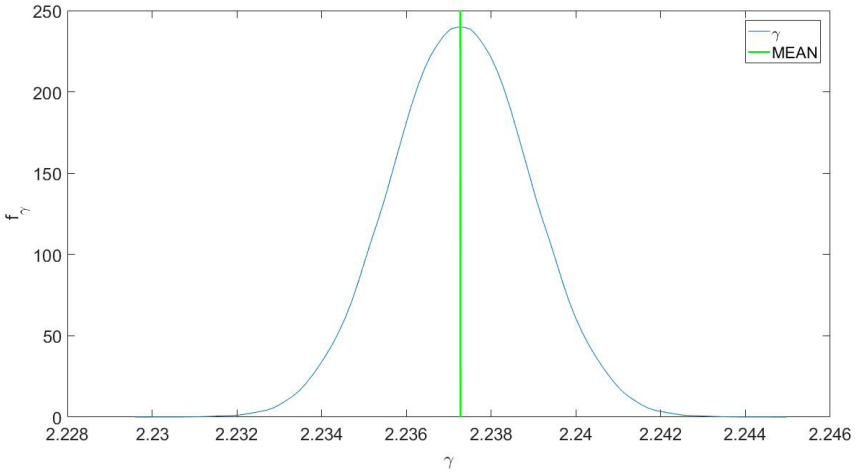

Figure 7. PDF of AlCrFeMoNbTaTiVW topological discrepancy (γ) with atomic radii modification, where "MEAN" stands for the mean value of γ.

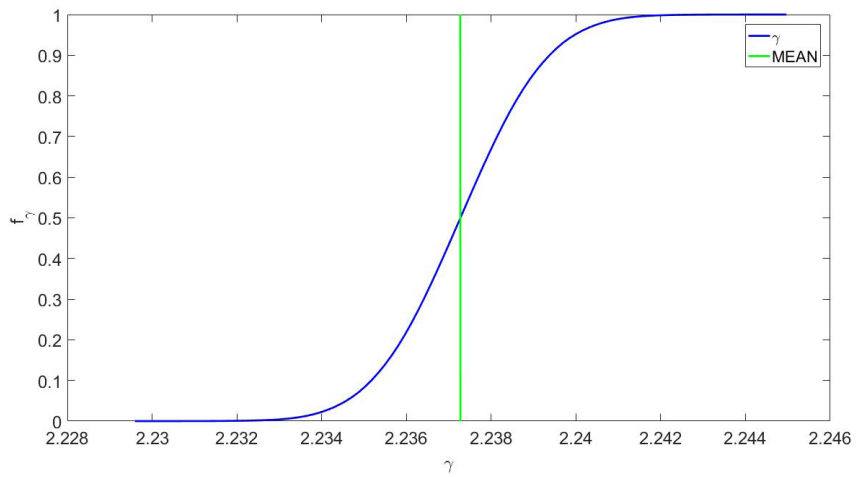

Figure 8. CDF of AlCrFeMoNbTaTiVW topological discrepancy (γ) with atomic radii modification, where "MEAN" stands for the mean value of γ.

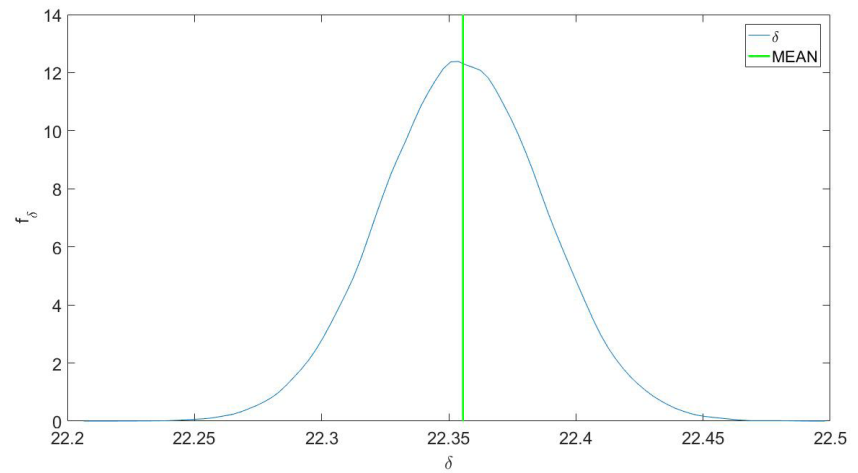

Figure 9. PDF of AlCrFeMoNbTaTiVW polydispersion of atomic radii (δ) with atomic radii modification, where "MEAN" stands for the mean value of δ.

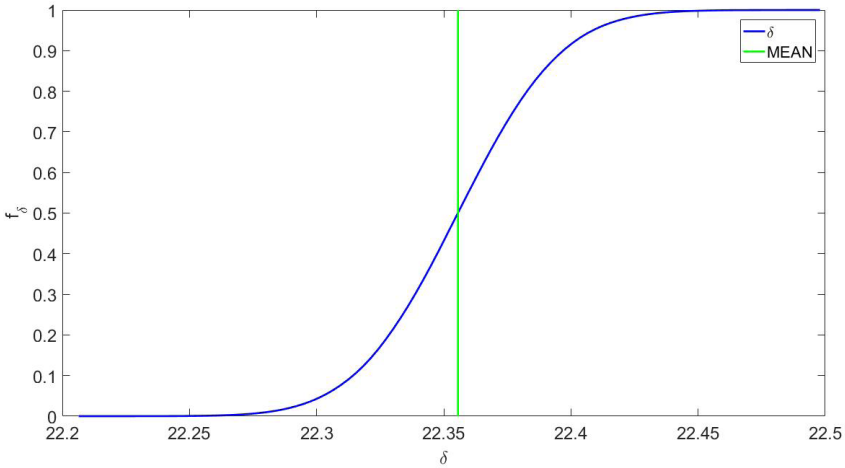

Figure 10. CDF of AlCrFeMoNbTaTiVW polydispersion of atomic radii (δ) with atomic radii modification, where "MEAN" stands for the mean value of δ.

Table 2. Input data for the alloy AlCrFeMoNbTaTiVW related to the UQ process, in which "LB" stands for lower bound, "std" standard deviation, and "UB" upper bound.

UIQ	Determ. (theoretical mean) (g)	Theoretical standard deviation (mg)	Simulated LB (g)	Simulated Mean (mg)	Simulated UB (g)	Simulated std (mg)	Relative error from mean (%)	Relative error from std (%)
m_{Al}	0.685	3.425	0.670	685.444	0.700	3.427	0.065	0.058
m_{Cr}	1.321	6.605	1.292	1320.929	1.350	6.604	-0.005	-0.015
m_{Fe}	1.419	7.095	1.387	1418.735	1.451	7.070	-0.019	-0.354
m_{Mo}	2.438	12.190	2.387	2437.550	2.493	12.130	-0.018	-0.495
m_{Nb}	2.360	11.800	2.301	2360.155	2.412	11.787	0.007	-0.110
m_{Ta}	4.597	22.985	4.500	4596.791	4.700	23.034	-0.005	0.213
m_{Ti}	1.216	6.080	1.186	1215.991	1.242	6.089	-0.001	0.148
m_{V}	1.294	6.470	1.267	1294.111	1.321	6.453	0.009	-0.263
m_{W}	4.670	23.350	4.571	4670.328	4.767	23.349	0.007	-0.004

In view of the uncertainty in the masses of the alloy components (according to Table 2), the previously planned and designed equimolar AlCrFeMoNbTaTiVW alloy turns out to be the non-equimolar alloy $Al_{0.690}Cr_{1.316}Fe_{1.398}Mo_{2.441}Nb_{2.341}Ta_{4.563}Ti_{1.218}V_{1.299}W_{4.634}$, for example, and the also non-equimolar alloy $Al_{0.685}Cr_{1.325}Fe_{1.418}Mo_{2.448}Nb_{2.355}Ta_{4.588}Ti_{1.220}V_{1.289}W_{4.636}$, among 99998 other alloys obtained via simulation in this investigation.

5.2. Statistical data of the problem

Table 2, Table 3, and Table 4 present several statistical data referring to the UIQs, SRQs without radii modification, and SRQs with modified atomic radii treated herein, respectively. Table 2 shows the masses of the alloy components involved in the alloy design. Observing Table 2, with respect to the mean, titanium mass presented the lowest relative error in absolute value, while aluminum mass showed the highest one. Related to the standard deviation, the tungsten mass presented the lowest relative error in absolute value, and molybdenum mass the highest one. The relative errors from the mean and from the standard deviation pointed out in Table 2 may serve as a quantification of the reliability of the input data. In the case of the reliability of the output data, the procedure adopted was to run the code 10 times with 1 x 10^5 realizations each. This procedure yielded a relatively low maximum absolute error of mean and standard deviation related to Ω of 0.004 and 3.210 x 10^{-4}, respectively, for example.

Table 3 and Table 4 address the eight parameters from the TPC and the mean radius of the alloy, highlighting that Table 4 presents only the parameters that differ from those in Table 3, i.e. the parameters not shown in Table 4 are already presented in Table 3. Two distinct types of data are compared by means of the relative error: theoretical and simulated. The relative errors calculated refer to the quantification of the convergence of the mean and the standard deviation of each UIQ and SRQ. The low values of the relative errors indicate a relatively good agreement between the theoretical proposed data and the simulated ones. This can be partially explained by the sufficient number of realizations selected, although a lower number of realizations already ensures enough precision to deal with this type of problem using LHS. This corroborates with the symmetry observed in Figure 4, Figure 6, Figure 8, and Figure 10. The lower and upper bounds, respectively LB and UB, are collected as the lowest and highest values simulated within each variable. Moreover, the coefficient of variation (CV) is presented in

Table 3. Output data for the alloy AlCrFeMoNbTaTiVW related to the UQ process without radii modification, in which "LB" stands for lower bound, "std" standard deviation, "UB" upper bound, and CV coefficient of variation.

SRQ	Determ.	Simulated LB	Simulated Mean	Simulated UB	Simulated std (10^{-4})	Relative error from mean (%)	CV (10^{-4})
Δr (%)	14.286	14.285	14.285	14.285	~0	5.593×10^{-11}	~0
γ	1.179	1.179	1.179	1.179	0.069	-1.631×10^{-6}	585.241
δ (%)	5.216	5.199	5.215	5.233	41.428	328.614×10^{-4}	7.944
V_M	5.333	5.323	5.333	5.343	22.351	2.451×10^{-4}	4.191
ΔS_{MIX} (J/kmol)	18.268	18.267	18.268	18.268	0.467	-5.104×10^{-4}	0.026
$\Delta\chi$	28.198	28.066	28.197	28.316	314.832	-1.407×10^{-3}	11.165
ΔH_{MIX} (kJ/mol)	-11.274	-11.354	-11.274	-11.183	202.307	2.388×10^{-4}	17.944
Ω	3.903	3.870	3.903	3.941	86.960	-7.003×10^{-4}	22.280
r_M (pm)	134.614	134.570	134.615	134.659	116.420	2.433×10^{-5}	0.864

Table 4. Output data affected by atomic radii modification for the alloy AlCrFeMoNbTaTiVW related to the UQ process, in which "LB" stands for lower bound, "std" standard deviation, "UB" upper bound, and CV coefficient of variation.

SRQ	Determ.	Simulated LB	Simulated Mean	Simulated UB	Simulated std	Relative error from mean (%)	CV (10^{-4})
Δr (%)	51.720	51.560	51.719	51.879	0.037	-0.002	7.154
γ	2.237	2.230	2.236	2.244	0.002	-0.045	8.944
δ (%)	22.356	22.220	22.355	22.490	0.032	-0.004	14.314
r_M (pm)	134.614	135.601	135.924	136.275	0.074	0.972	5.445

the last column of Table 3 and Table 4. In the case with no radii modification (Table 3), Δr and γ presented the lowest and the highest dispersions, respectively. The modified radii case (Table 3 and Table 4) showed ΔS_{MIX} and Ω as the lowest and highest dispersive parameters, respectively.

The reliability of the obtained results may be verified by observing Table 3 (without radii modification), in which the deterministic and probabilistic values of γ and $\Delta\chi$ do not attend their respective criteria to SSF, while the values of the other six parameters are within each range to SSF. In the case of radii modification (Table 4), only ΔS_{MIX}, ΔH_{MIX}, and Ω comply with SSF, while the other five parameters are out of their accepted ranges to SSF. Comparing the deterministic and simulated values between Table 3 and Table 4, it can be noted that the SRQs dependent on atomic radii (Δr, γ, δ, and r_M) did not attend the related criteria previously established. As a result of going from 6 criteria met (without radii modification) for the SSF to only 3 (with radii modification), in addition to not fulfilling all the radii-dependent SSF criteria, the atomic radii modification theory proved to be non-effective in the application in TPC approach (modified TPC) for the tested alloy AlCrFeMoNbTaTiVW. In other words, if the associated criteria do not change in its formulation when the atomic radii are modified, the SSF criteria will not be fulfilled in 5 out of 8 criteria for the alloy presented herein.

In what refers only to the parameter γ, for example, while the alloy $Al_{0.690}Cr_{1.316}Fe_{1.398}Mo_{2.441}Nb_{2.341}Ta_{4.563}Ti_{1.218}V_{1.299}W_{4.634}$ corresponds to solid solution formation, $Al_{0.685}Cr_{1.325}Fe_{1.418}Mo_{2.448}Nb_{2.355}Ta_{4.588}Ti_{1.220}V_{1.289}W_{4.636}$ does not form solid solution per classical TPC. This almost residual difference between the two multicomponent alloys which could happen depending on the adopted manufacturing route, determines whether SSF effectively occurs. In other words, in the same batch, under the proposed uncertainty framework context, some samples of this alloy can result in SSF, others not.

Figure 11 through Figure 16 present several possible graphical sensitivity analyses (SAs) aiming at pictorially analyzing the influence of some UIQs on some SRQs (Figures 11-16). Figure 11 through Figure 13 picture the influence of the mean atomic radius of the alloy on atomic radii difference (Δr), polydispersion of atomic radii (δ), and topological discrepancy (γ), respectively. Figure 14, Figure 15, and Figure 16 show the impact of the mass of aluminum (for example) on Δr, δ, and γ, respectively. In the case of process improvement initiatives, these mappings may aid in future dispersion reduction, if possible.

In addition to the scatter plots already mentioned (qualitative analysis), a quantitative analysis is performed via Pearson correlation coefficients comparison, in which Table 5 presents the correlation coefficients between the UIQs (masses of the alloy components involved in the alloy design) and all the SRQs (the parameters and the mean radius of the elements involved) of the problem in the condition without atomic radii modification. By observing Table 5, it is possible to note that: (a) Δr is almost not influenced by the masses of the alloy components; (b) although very low, the influence of chromium mass on γ is the highest; (c) in the case of δ, iron mass has the highest impact, such that to lower the value of δ, it is recommended to lower the iron mass; (d) V_M is also most influenced by titanium and tungsten masses, however the influence is low; (e) the highest impact on ΔS_{MIX} comes from vanadium mass; (f) in the case of $\Delta\chi$, the most impactful UIQ is the tungsten mass; (g) aluminum mass influences ΔH_{MIX} the most; (h) Ω is mostly affected by aluminum mass; and (i) chromium mass is the most influencing UIQ on r_M, however in a low level.

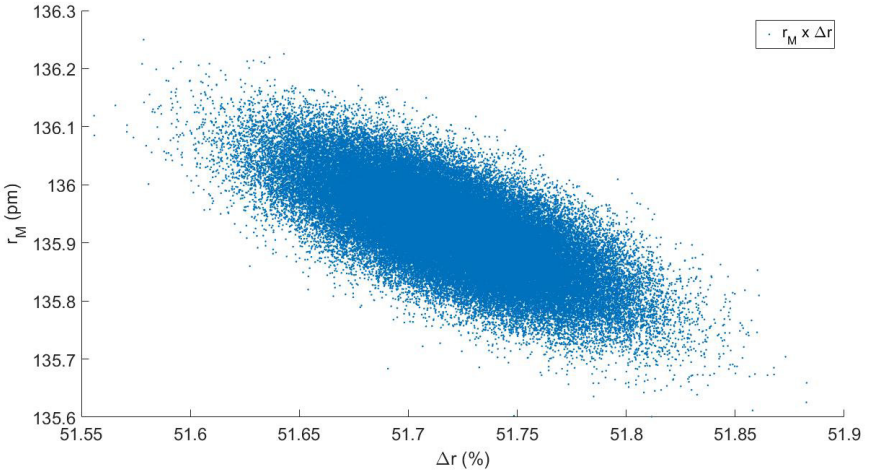

Figure 11. Scatter plot of r_M *vs.* Δr of AlCrFeMoNbTaTiVW.

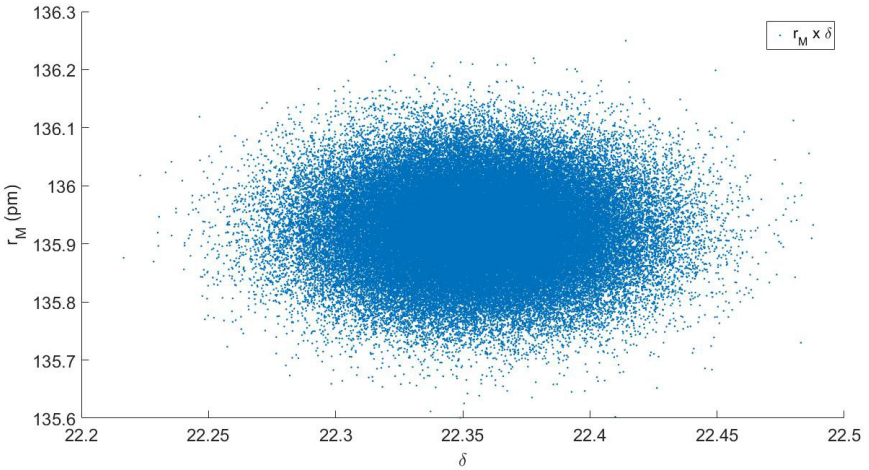

Figure 12. Scatter plot of r_M *vs.* δ of AlCrFeMoNbTaTiVW.

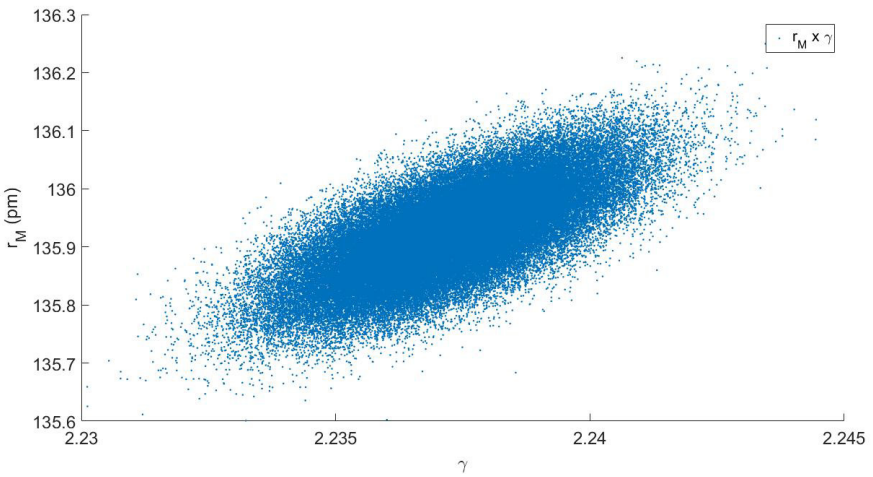

Figure 13. Scatter plot of r_M *vs.* γ of AlCrFeMoNbTaTiVW.

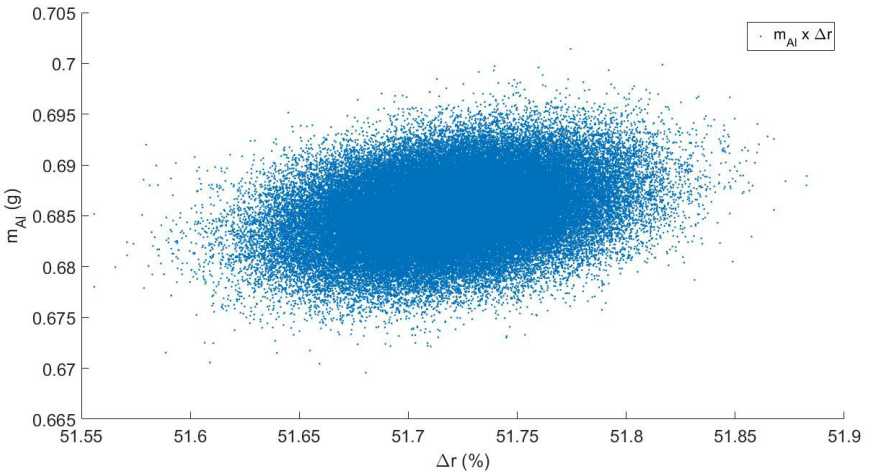

Figure 14. Scatter plot of m_{Al} *vs.* Δr of AlCrFeMoNbTaTiVW.

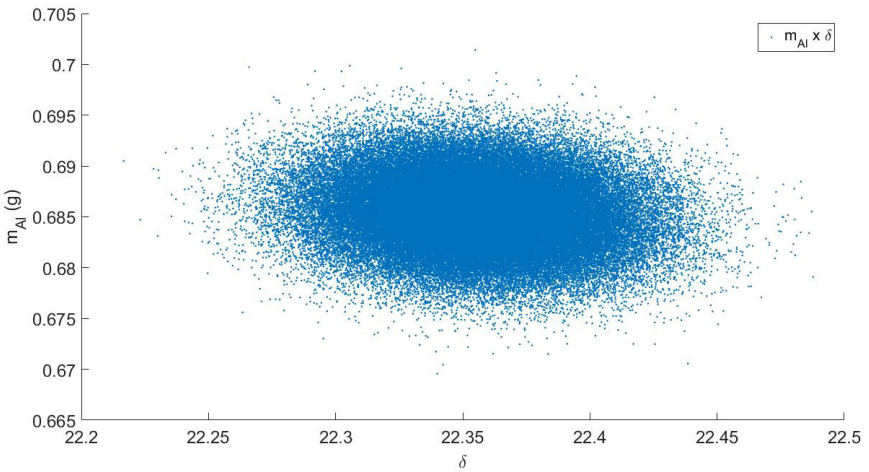

Figure 15. Scatter plot of m_{Al} *vs.* δ of AlCrFeMoNbTaTiVW.

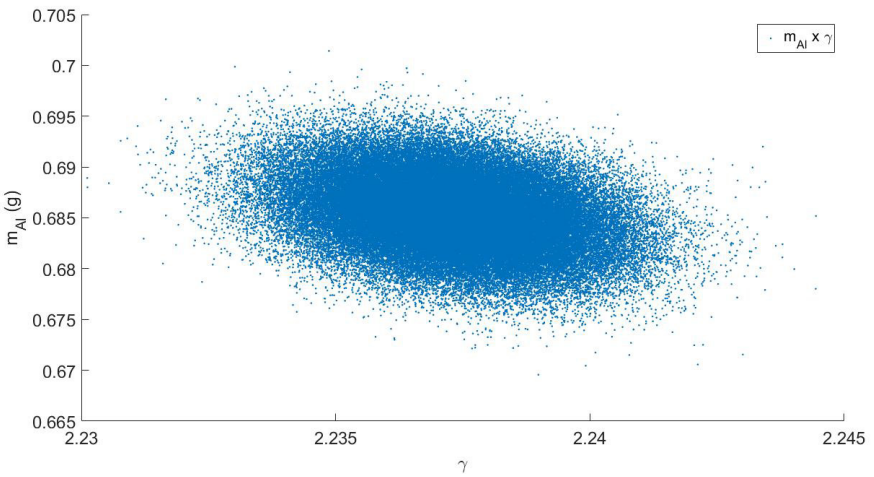

Figure 16. Scatter plot of m_{Al} *vs.* γ of AlCrFeMoNbTaTiVW.

Under another perspective, the following list describes which SRQ is the most influenced by each UIQ. From Table 5: (a) aluminum mass influences more Ω than any other SRQ; (b) chromium mass has its highest influence on δ; (c) iron mass affects δ the most; (d) molybdenum mass has its highest impact on ΔH_{MIX}; (e) niobium mass has its highest influence on $\Delta\chi$; (f) tantalum mass has its highest impact on Ω; (g) titanium mass has its highest influence on Ω; (h) vanadium has its highest impact on ΔH_{MIX}; and (i) tungsten mass affects $\Delta\chi$ the most.

In the case of atom radii modification and regarding only the SRQs with the radii in their formulation, as per Table 6: (a) Δr is most influenced by the iron mass; (b) γ is also most impacted by iron mass; (c) δ is most affected by the iron mass (specifically, it is the highest correlation coefficient overall); and (d) although low, r_M is most influenced by titanium mass.

In the other way, yet per Table 6: (a) aluminum mass has its highest influence on both Δr and γ; (b) chromium mass has its highest influence concomitantly on Δr and γ; (c) iron mass affects δ the most; (d) molybdenum mass has its highest influence on δ; (e) niobium mass has its highest impact on δ; (f) tantalum mass has its highest influence on δ; (g) titanium has its highest impact concomitantly on Δr and γ; (h) vanadium has its highest influence on δ; and (i) tungsten has its highest impact on δ.

An important result in the context of this research refers to the overall impact of the masses of the alloy components on the addressed parameters. This influence was quantified here by the impact factor, which refers to the summation of the absolute values of Pearson correlation coefficients. Table 7 shows each alloy component mass ranked by impact factor. Per classical TPC approach (without atomic radii modification), the tungsten mass is the most influential and tantalum mass is the less one, while per modified TPC approach (with radii modification) tantalum keeps on being the least influential and now the most influential is the aluminum mass. Table 7 also presents the percent variation of modified TPC related to classical TPC, in which in 7 out of 9 masses the trend is to increase the impact factor when the atomic radii is modified.

Therefore, the Pearson correlation coefficients mapping, made in Table 5 and Table 6, may serve as a guide toward the SSF by means of changing the molar fraction of the most impactful alloy elements aiming to reach SSF related to all the parameters and associated criteria.

Table 5. Pearson correlation coefficients between UIQs and SRQs addressed in AlCrFeMoNbTaTiVW design without atomic radii modification.

	Δr (%)	γ	δ (%)	V_M	ΔS_{MIX} (J/kmol)	$\Delta\chi$	ΔH_{MIX} (kJ/mol)	Ω	r_M (pm)
m_{Al} (g)	9.387 x 10^{-13}	-0.002	-0.235	0.001	0.001	-0.175	-0.755	-0.760	0.002
m_{Cr} (g)	0.477 x 10^{-13}	-0.006	0.291	0.004	-0.002	-0.214	0.221	0.154	0.006
m_{Fe} (g)	-4.533 x 10^{-13}	0.003	0.743	0.001	0.002	-0.235	-0.211	-0.233	-0.003
m_{Mo} (g)	2.638 x 10^{-13}	-0.003	-0.355	-0.002	0.006	0.242	0.361	0.340	0.003
m_{Nb} (g)	-6.428 x 10^{-13}	0.001	-0.011	0.002	0.001	-0.155	-0.055	-0.007	-0.001
m_{Ta} (g)	7.077 x 10^{-13}	0.001	-0.006	-0.003	-0.002	-0.025	-0.044	0.058	-0.001
m_{Ti} (g)	-8.020 x 10^{-13}	-0.005	0.105	-0.005	0.001	-0.092	-0.117	-0.143	0.005
m_V (g)	0.603 x 10^{-13}	0.004	-0.202	0.001	0.008	-0.188	0.261	0.186	-0.004
m_W (g)	-3.212 x 10^{-13}	0.001	-0.351	-0.005	-0.001	0.860	0.341	0.409	-0.001

Table 6. Pearson correlation coefficients between UIQs and SRQs affected by atomic radii modification in AlCrFeMoNbTaTiVW design.

	Δr (%)	γ	δ (%)	r_M (pm)
m_{Al} (g)	0.314	-0.314	-0.132	0.001
m_{Cr} (g)	-0.095	0.095	-0.068	-0.001
m_{Fe} (g)	-0.362	0.362	0.918	0.001
m_{Mo} (g)	-0.087	0.087	-0.196	0.001
m_{Nb} (g)	0.053	-0.053	-0.155	-0.004
m_{Ta} (g)	0.050	-0.050	0.061	-0.001
m_{Ti} (g)	0.174	-0.174	-0.150	0.006
m_V (g)	0.044	-0.044	-0.193	0.002
m_W (g)	-0.093	0.093	-0.104	0.004

Table 7. Comparison of the impact factors with and without atomic radii modification of the masses of the alloy components in AlCrFeMoNbTaTiVW.

Mass of the alloy element	Impact factor (without atomic radii modification)	Rank (without atomic radii modification)	Impact factor (with atomic radii modification)	Rank (with atomic radii modification)	Percent variation (%)
m_{Al}	1.931	2	2.453	1	27.033
m_{Cr}	0.898	5	0.854	7	-4.900
m_{Fe}	1.431	3	2.325	2	62.474
m_{Mo}	1.312	4	1.322	4	0.762
m_{Nb}	0.233	8	0.485	8	108.155
m_{Ta}	0.140	9	0.294	9	110.000
m_{Ti}	0.473	7	0.862	6	82.241
m_{V}	0.854	6	0.927	5	8.548
m_{W}	1.969	1	1.910	3	-2.996

6. Conclusions

This paper presented an uncertainty quantification (UQ) analysis conducted over the thermophysical parameters calculation (TPC) approach to check the behavior of the parameters (system response quantities, SRQs) as the masses of the alloy elements involved vary and their atomic radii are modified (uncertain input quantities, UIQs). Among the 8 parameters and their associated criteria that were addressed to predict the solid solution formation (SSF), 2 are only radii dependent, 1 is concomitantly dependent on radii and masses, and the remaining ones are dependent only on masses. In the strategy proposed by the presented UQ framework, the UIQs are Gaussian aleatory-type and Latin hypercube sampling (LHS) was the selected method to propagate the uncertainty through the mathematical model presented. The AlCrFeMoNbTaTiVW alloy was subjected to the proposed framework, generating probabilistic distributions, graphical sensitivity analyses, relative errors, and Pearson correlation coefficients as the main results.

According to the research conducted herein, the main conclusions are the following: (a) the UQ framework conducted over TPC can generate a range of results related to SSF according to the input data; (b) in an uncertain paradigm, a previous equimolar HEA turns out now to be a near-equimolar HEA; (c) for each SRQ there is at least one UIQ as the most impactful. In case of computational burden, the most influencing UIQs should be designed toward the establishment of an SSF, if it is the design objective; (d) it is not recommended to apply the atomic radii modification theory in TPC due to the lack of support of the mathematical formulation in a reasonable manner; (e) if a HEA is designed near the boundaries of SSF acceptance in the criteria, some samples of the same batch of the HEA may result in SSF, and other samples may not.

In view of these conclusions, there is still an increasing demand toward the knowledge of prediction of SSF in HEAs' design. The UQ framework and the parameters applied herein compose just a minor branch in the vast universe of HEAs' design. In this scenario, uncertainty quantification methods may help in HEAs' design, mainly regarding avoiding unnecessary experiments and unexpected properties of the alloys.

7. Acknowledgements

The authors would acknowledge the journal for the opportunity to share this work. The authors would also acknowledge the following research councils for the financial support: (a) CNPQ (proj. 408406/2021-6), (b) CatalisaICT SEBRAE (proj. 29083*128), and (c) FAPESP (proj. 2023/09818-8).

8. References

1. Razuan R, Jani NA, Harun MK, Talari MK. Microstructure and hardness properties investigation of Ti and Nb added FeNiAlCuCrTixNby high entropy alloys. Trans Indian Inst Met. 2013;66(4):309-12. http://doi.org/10.1007/s12666-013-0265-7.
2. Shun T-T, Chang L-Y, Shiu M-H. Microstructures and mechanical properties of multiprincipal component CoCrFeNiTix alloys. Mater Sci Eng A. 2012;556:170-4. http://doi.org/10.1016/j.msea.2012.06.075.
3. Yeh J-W, Chen S-K, Lin S-J, Gan J-Y, Chin T-S, Shun T-T, et al. Nanostructured high-entropy alloys with multiple principal elements: novel alloy design concepts and outcomes. Adv Eng Mater. 2004;6(5):299-303. http://doi.org/10.1002/adem.200300567.
4. Cantor B, Chang ITH, Knight P, Vincent AJB. Microstructural development in equiatomic multicomponent alloys. Mater Sci Eng A. 2004;375-377:213-8. http://doi.org/10.1016/j.msea.2003.10.257.
5. Zhang Y, Wen C, Dang P, Lookman T, Xue D, Su Y. Toward ultra-high strength high entropy alloys via feature engineering. J Mater Sci Technol. 2024;200:243-52. http://doi.org/10.1016/j.jmst.2024.02.058.
6. Restivo TAG, Nonato RBP, Rossoni RF, Ferreira OA, Padovani C, Aranha N, et al. Sintering of metallic diamond alloy powders. J Therm Anal Calorim. 2023;148(23):13003-9. http://doi.org/10.1007/s10973-023-12260-8.
7. Restivo TAG, Restivo GMG. Development of ultra-hard multi-component alloys. J Mater Res. 2021;36(6):1316-27. http://doi.org/10.1557/s43578-021-00195-5.
8. Juan C-C, Tseng K-K, Hsu W-L, Tsai MH, Tsai C-W, Lin C-M, et al. Solution strengthening of ductile refractory HfMoxNbTaTiZr high-entropy alloys. Mater Lett. 2016;175:284-7. http://doi.org/10.1016/j.matlet.2016.03.133.
9. Fan X, Chen S, Steingrimsson B, Xiong Q, Li W, Liaw PK. Dataset for fracture and impact toughness of high-entropy alloys. Sci Data. 2023;10(1):37. http://doi.org/10.1038/s41597-022-01911-4. PMid:36658125.

10. Zeng C, Neils A, Lesko J, Post N. Machine learning accelerated discovery of corrosion-resistant high-entropy alloys. Comput Mater Sci. 2024;237:112925. http://doi.org/10.1016/j.commatsci.2024.112925.
11. Du YJ, Xu SM, Wang F, Li JL, Wen GD, Xiong JT, et al. Simultaneously enhancing strength-ductility synergy in refractory high entropy alloys by a heterogeneous structure design. J Alloys Compd. 2024;993:174550. http://doi.org/10.1016/j.jallcom.2024.174550.
12. Peng Z, Li B, Luo Z, Chen X, Tang Y, Yang G, et al. A lightweight AlCrTiV0,5Cux high-entropy alloy with excellent corrosion resistance. Materials. 2023;16(7):2922. http://doi.org/10.3390/ma16072922. PMid:37049215.
13. Brotzu A, De Filippo B, Natali S, Zortea L. High Entropy Cantor Alloys (HEAs) modification induced by tungsten alligation, heat treatment and deep cold plastic deformation. Frat. Integrita Strutt. 2023;63:309-20.
14. Ren X, Li Y, Qi Y, Wang B. Review on preparation technology and properties of refractory high entropy alloys. Materials. 2022;15(8):2931. http://doi.org/10.3390/ma15082931. PMid:35454623.
15. King DJM, Middleburgh SC, McGregor AG, Cortie MB. Predicting the formation and stability of single phase high-entropy alloys. Acta Mater. 2016;104:172-9. http://doi.org/10.1016/j.actamat.2015.11.040.
16. Zhang F, Zhang C, Chen SL, Zhu J, Cao WS, Kattner UR. An understanding of high entropy alloys from phase diagram calculations. Calphad. 2014;45:1-10. http://doi.org/10.1016/j.calphad.2013.10.006.
17. Senkov ON, Miller JD, Miracle DB, Woodward C. Accelerated exploration of multi-principal element alloys with solid solution phases. Nat Commun. 2015;6(1):6529. http://doi.org/10.1038/ncomms7529. PMid:25739749.
18. Miracle DB, Senkov ON. A critical review of high entropy alloys and related concepts. Acta Mater. 2017;122:448-511. http://doi.org/10.1016/j.actamat.2016.08.081.
19. Kucza W. High entropy alloys and thermodynamically derived high stability alloys; a compositional comparative study of all 3-7 element systems composed of ten 3d metals at 1273 K. J Alloys Compd. 2022;894:162443. http://doi.org/10.1016/j.jallcom.2021.162443.
20. Divinski SV, Pokoev AV, Esakkiraja N, Paul A. A mystery of "sluggish diffusion" in high-entropy alloys: the truth or a myth? Diffusion Foundations. 2018;17:69-104. http://doi.org/10.4028/www.scientific.net/DF.17.69.
21. He Q, Yang Y. On lattice distortion in high entropy alloys. Front Mater. 2018;5:42. http://doi.org/10.3389/fmats.2018.00042.
22. Liu X, Duan Y, Yang X, Huang L, Gao M, Wang T. Enhancement of magnetic properties in FeCoNiCr0.4CuX high entropy alloys through the cocktail effect for megahertz electromagnetic wave absorption. J Alloys Compd. 2021;872:159602. http://doi.org/10.1016/j.jallcom.2021.159602.
23. Chou TH, Huang JC, Yang CH, Lin SK, Nieh TG. Consideration of kinetics on intermetallics formation in solid-solution HEAs. Acta Mater. 2020;195:71-80. http://doi.org/10.1016/j.actamat.2020.05.015.
24. Ren M-X, Li BS, Fu H-Z. Formation condition of solid solution type high-entropy alloy. Trans Nonferrous Met Soc China. 2013;23(4):991-5. http://doi.org/10.1016/S1003-6326(13)62557-1.
25. Li J-H, Tsai M-H. Theories for predicting simple solid solution HEAs: classification, accuracy, and important factors impacting accuracy. Scr Mater. 2020;188:80-7. http://doi.org/10.1016/j.scriptamat.2020.06.064.
26. Gao MC, Alman DE. Searching for next single-phase high-entropy alloy compositions. Entropy. 2013;15(10):4504-19. http://doi.org/10.3390/e15104504.
27. Xie L, Brault P, Thomann A-L, Bauchire J-M. AlCoCrCuFeNi high-entropy alloy cluster growth and annealing on silicon: A classical molecular dynamics simulation study. Appl Surf Sci. 2013;285P:810-6. http://doi.org/10.1016/j.apsusc.2013.08.133.
28. Zhang C, Zhang F, Chen S, Cao W. Computational thermodynamics aided high-entropy alloy design. J Miner Met Mater Soc. 2012;64(7):839-45. http://doi.org/10.1007/s11837-012-0365-6.
29. Zhang F, Zhang C, Chen SL, Zhu J, Cao WS, Kattner UR. An understanding of high entropy alloys from phase diagram calculations. Calphad. 2014;45:1-10. http://doi.org/10.1016/j.calphad.2013.10.006.
30. Nazir T, Shaukat N, Tariq NUH, Shahid RN, Bhatti MH. A comprehensive strategy for phase detection of high entropy alloys: machine learning and deep learning approaches. Mater Today Commun. 2023;37:107525. http://doi.org/10.1016/j.mtcomm.2023.107525.
31. Wang Y, Liu H, Hao X, Yang C, Liu Y, Chen L, et al. First-principles calculations to investigate phase stability, elastic and thermodynamic properties of TiMoNbX (X=Cr, Ta, Cr and Ta) refractory high entropy alloys. J Phys Condens Matter. 2024;36(48):485902. http://doi.org/10.1088/1361-648X/ad7437. PMid:39191269.
32. Cagirici M, Wang P, Ng FL, Nai MLS, Ding J, Wei J. Additive manufacturing of high-entropy alloys by thermophysical calculations and *in situ* alloying. J Mater Sci Technol. 2021;94:53-66. http://doi.org/10.1016/j.jmst.2021.03.038.
33. Poonia A, Kishor M, Ayyagari KPR. Designing of high entropy alloys with high hardness: a metaheuristic approach. Sci Rep. 2024;14(1):7692. http://doi.org/10.1038/s41598-024-57094-y. PMid:38565897.
34. Wang Z, Huang Y, Liu CT, Li J, Wang J. Atomic packing and size effect on the Hume-Rothery rule. Intermetallics. 2019;109:139-44. http://doi.org/10.1016/j.intermet.2019.04.001.
35. Batt GM. Investigation of the spectral properties of disordered alloys and superconductors [thesis]. Bristol: University of Bristol; 2008.
36. Yang X, Zhang Y. Prediction of high-entropy stabilized solid-solution in multicomponent alloys. Mater Chem Phys. 2012;132(2-3):233-8. http://doi.org/10.1016/j.matchemphys.2011.11.021.
37. Singh KA, Kumar N, Dwivedi A, Subramaniam A. A geometrical parameter for the formation of disordered solid solutions in multi-component alloys. Intermetallics. 2014;53:112-9. http://doi.org/10.1016/j.intermet.2014.04.019.
38. Guo S, Ng C, Lu J, Liu CT. Effect of valence electron concentration on stability of fcc or bcc phase in high entropy alloys. J Appl Phys. 2011;109(10):103505. http://doi.org/10.1063/1.3587228.
39. Li A, Zhang X. Thermodynamic analysis of the simple microstructure of AlCrFeNiCu HEA with multi-principal elements. Acta Metall Sin. 2009;22(3):219-24. http://doi.org/10.1016/S1006-7191(08)60092-7.
40. Li C, Li JC, Zhao M, Jiang Q. Effect of alloying elements on microstructure and properties of multi-principal elements high-entropy alloys. J Alloys Compd. 2009;475(1-2):752-7. http://doi.org/10.1016/j.jallcom.2008.07.124.
41. Yang X, Zhang Y. Prediction of high-entropy stabilized solid-solution in multicomponent alloys. Mater Chem Phys. 2012;132(2-3):233-8. http://doi.org/10.1016/j.matchemphys.2011.11.021.
42. Fang S, Xiao X, Xia L, Li W, Dong Y. Relationship between the widths of supercooled liquid regions and bond parameters of Mg-based bulk metallic glasses. J Non-Cryst Solids. 2013;321(1-2):120-5. http://doi.org/10.1016/S0022-3093(03)00155-8.
43. Takeuchi A, Inoue A. Calculations of amorphous-forming composition range for ternary alloy systems and analyses of stabilization of amorphous phase and amorphous-forming ability. Mater Trans. 2011;7:1435-44.
44. Ye YF, Wang Q, Lu J, Liu CT, Yang Y. Design of high entropy alloys: a single-parameter thermodynamic rule. Scr Mater. 2015;104:53-5. http://doi.org/10.1016/j.scriptamat.2015.03.023.
45. Tsekov R. Hard spheres model of the atom. Chemistry. 2015;24:818-24.

46. Hu Q, Guo S, Wang JM, Yan YH, Chen SS, Lu DP, et al. Parametric study of amorphous HEAs formation from two new perspectives: atomic radius modification and crystalline structure of alloying elements. Sci Rep. 2017;7(1):39917. http://doi.org/10.1038/srep39917. PMid:28051186.
47. Oberkampf WL, Roy CJ. Verification and validation in scientific computing. Cambridge: Cambridge University Press; 2010.
48. Nonato RBP. Multi-level uncertain fatigue analysis of a truss under incomplete available information. Frat. Integrita Strutt. 2023;65(66):17-37. http://doi.org/10.3221/IGF-ESIS.66.02.
49. Nonato RBP. Bi-level hybrid uncertainty quantification in fatigue analysis: S-N curve approach. Frat. Integrita Strutt. 2020;54(54):88-103. http://doi.org/10.3221/IGF-ESIS.54.06.
50. Ghanem R, Higdon D, Owhadi H. Handbook of uncertainty quantification. Cham: Springer; 2017.
51. Fall A, Grasinger M, Dayal K. An optimized species-conserving Monte Carlo method with potential applicability to high entropy alloys. Comput Mater Sci. 2023;217(8):111886. http://doi.org/10.1016/j.commatsci.2022.111886.
52. Jank W. Quasi-Monte Carlo sampling to improve the efficiency of Monte Carlo EM. Comput Stat Data Anal. 2005;48(4):685-701. http://doi.org/10.1016/j.csda.2004.03.019.
53. Lu Z, Zhou C, Song Z, Song S. Subset simulation-based method for cumulative distribution function sensitivity of output response in random environment. Proc Inst Mech Eng, C J Mech Eng Sci. 2012;226(11):2770-90. http://doi.org/10.1177/0954406212436444.
54. Branicki M, Majda AJ. Fundamental limitations of polynomial chaos for uncertainty quantification in systems with intermittent instabilities. Commun Math Sci. 2013;11(1):55-103. http://doi.org/10.4310/CMS.2013.v11.n1.a3.
55. Edalatpanah SA. Multidimensional solution of fuzzy linear programming. PeerJ Comput Sci. 2023;9:e1646. http://doi.org/10.7717/peerj-cs.1646. PMid:38077581.
56. Lee S, Lyu H, Hwang I. Analytical uncertainty propagation for satellite relative motion along elliptic orbits. J Guid Control Dyn. 2016;39(7):1593-601. http://doi.org/10.2514/1.G001848.
57. Zhao K, Xue H, Yang F, Zhao L. Probability prediction of crack growth rate of environmentally assisted cracks of nickel-based alloys based on Latin hypercube sampling. Int J Press Vessels Piping. 2019;172:391-6. http://doi.org/10.1016/j.ijpvp.2019.04.005.
58. Nonato RBP, Restivo TAG. The effect of atomic radius modification on topological parameters of high-entropy alloys. In: I Seven International Engineering Congress; 2024 Apr 8-9; Itupeva, SP, Brazil. Proceedings. São José dos Pinhais: Seven Publications Company; 2024. http://doi.org/10.56238/sevenIengineering-006.